Using abstract waveforms to infer gravitational wave source properties with machine learning

Julianna Levanti, Ryan Magee
LIGO Caltech SURF Pre-Proposal

The LIGO-Virgo-KAGRA collaboration provides low-latency (near-real time) localization using the signal-to-noise ratio measured for a single point in the search parameter space. Parameter estimation pipelines subsequently samples the full parameter space to obtain more accurate estimates of the localization. However, this process is computationally expensive. The multi-messenger detection of the binary neutron star merger GW170817 confirmed the need for accurate and fast data products. Some detection pipelines utilize singular value decomposition to reduce the filtering cost. This project uses machine learning to input signal-to-noise ratios from singular value decomposition time-series into a simulation-based inference (SBI), a likelihood free inference algorithm, which outputs a posterior with an accurate parameter estimation, such as a sky map, to localize compact binary coalescences and infer other source properties.

I. INTRODUCTION

Gravitational Waves (GWs) were first detected in 2015 by the Laser Interferometer Gravitational-Wave Observatory (LIGO) [1]. GWs are physical ripples in the fabric of space and time, stretching and compressing space. GWs originate from compact binary coalescence (CBC), the inspiral and merge of two extremely massive objects such as black holes or neutron stars. GWs can also originate from other exotic events in the universe, such as supernovae, but this project will focus solely on CBCs. GWs can be detected by laser interferometers such as LIGO, which uses laser interference to measure the impact of passing GWs [1]. Information encoded in the GWs signal detected by LIGO can give scientists valuable information about each source, like distance and location.

The first binary neutron star merger, detected by LIGO in August 2017 [2], was a breakthrough for our understanding of astrophysics. The Europeans Space Agency's INTEGRAL telescope and NASA's Fermi Gamma-ray Space telescope observed a brief gamma-ray burst from the source [3]. The Hubble Space Telescope and The Chandra X-ray Telescope also detected electromagnetic (EM) radiation from the same direction [3]. Further evidence shows that the James Webb Space Telescope detected mid-infrared emission of exotic heavy-element tellurium [4]. Analysis of the GW data and the EM counterparts support that the progenitor was most likely a binary neutron star merger. The event is important for our understanding of the universe due to its GW and EM counter parts [2, 5, 6]. Studies have shown efforts towards low-latency GW detection [7]. This project aims to improve the accuracy of our super-low-latency data products.

Filtering analysis computes a comparison between a large number of modeled CBC waveforms (Figure 1) and the detector output to produce a signal-to-noise ratio (SNR). SNRs can contain GW signals from compact binaries covered by background noise [8]. The data set in Figure 1 contains waveforms accounting for a variety of masses and spins, which encompasses information about source parameters, but seem to look similar in appearance.

GW data from CBCs are dependant on a high number of physical dimensions, such as mass, spin, distance, and inclination. Previous studies face issues in quantifying these dimensions due to the high parameter space [9–11]. GW strain observed on earth depends on an array of 15 parameters. The parameters are as followed: mass of the primary object, mass of the secondary object, luminosity distance, the integration constant, time of coalescence, position of ascension, position of declination, inclination, polarization angle, the spin, angle, and orientation of the primary object, and the spin, angle, and orientation of the secondary object [12]. It is difficult to apply these methods over a fixed sample of data, as well as a fixed number of dimensions to attain quality results [11], hence the extreme efforts and costs full parameter estimation process require. However, LIGO is able to create low-latency sky maps and measure SNRs by imposing constraints on the signal parameter space.

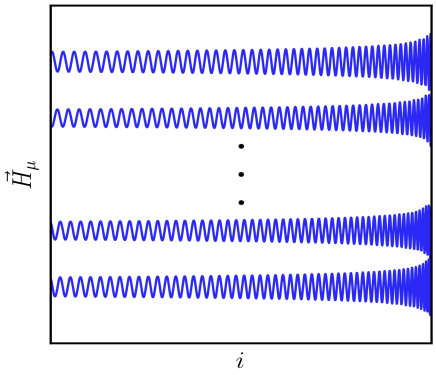

FIG. 1: Simulated waveform candidates. $\vec{H}_\mu$ is an unit-less measurement, referred to as strain. Strain is the fractional change in distance the lasers are stretched or compressed by a passing gravitational wave, relative to the original length.

A. Singular Value Decomposition

We plan to generate sky maps more efficiently and accurately by using singular value decomposition (SVD) (Equation 1) on original waveforms and mapping them

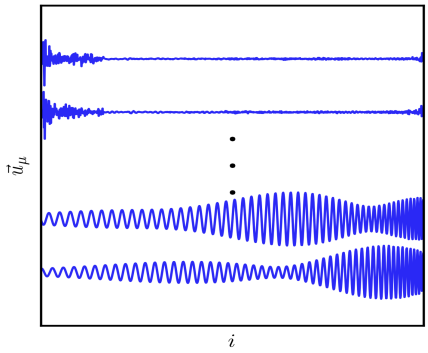

FIG. 2: The result of abstract waveforms computed through SVD using original gravitational waveforms.

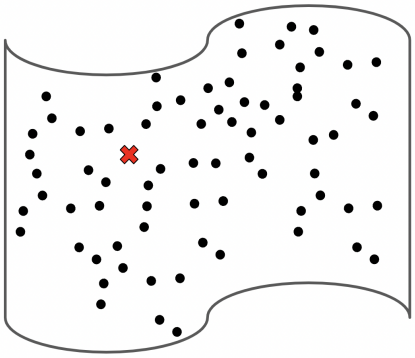

FIG. 3: The figure represents pre-SVD modeled waveforms under a parameter space. The red X indicates a waveform that can be created with the SVD waveforms extracted from the space with high accuracy.

onto an abstract parameter space. Original waveforms can be transformed through SVD which reduces the amount of GW filtering required to analyze a given region of a parameter space of compact binary coalescence [13].

In Equation 1, h are the GW time series, a are reconstruction coefficients, and u are SVD abstract basis vectors, all indexed by μ [13]. Equation 2 represents SNR, ρ, which is equal to the noise-weighted inner product of a waveform template and raw strain data, d. Substituting Equation 1 in for h, we are able to use distributive properties and replace the new inner product with the SVD SNR, Q, shown in Equation 3, and create SNR Equation 4, which can be compared similarly with Equation 1.

$$h = \sum a_\mu u^\mu \tag{1}$$

$$\rho =< h|d > \tag{2}$$

$$Q =< u|d > \tag{3}$$

$$\rho = \sum a_\mu Q^\mu \tag{4}$$

Equation 1 is a breakdown of each waveform template into SVD basis vectors, where as Equation 4 is a breakdown of each original SNR into SVD SNRs. SVD basis vectors (Figure 2) are abstract and do not contain any concrete evidence regarding dimensions we hope to reveal. All of the abstract waveforms are orthogonal and do not overlap with one another [9, 10].

B. Machine Learning

The modeled waveforms represented in Figure 1 can be compiled into a parameter space shown in Figure 3, where each point represents an individual template. Computing abstract waveforms from SVD that will fit in the gaps of the sample space in Figure 2 through a neural network is an example of how apply machine learning. A specific number of SVDs can be added together in various ways to create each template in the space. The quantity of SVDs can vary from 5 to 100 depending on the characteristics of the space. Low-latency sky maps are created by selecting one template. Since the empty space compares to the plotted templates with high accuracy, it is possible to cover more area in the space by using the SVDs instead of just a single waveform. This means that we can cover a larger area of the template space by using the set number of SVDs that correspond to the waveforms in that space.

Computationally comparing SVD waveforms with original waveforms can be an extensive process. Instead of waiting to map the SVD for comparison with the original waveforms, our project looks to input the abstract waveforms through a neural network to compute a likelihood of the physical properties of a GW source. Normally, posterior probability distribution calculations are done after a gravitational wave is detected. Using simulation based inference, machine learning can help us "front-load" the expensive computations to build a posterior and calculate likelihood of parameters, given previously detected parameters. The use of a neural network has been confirmed and tested as a reliable structure for a machine learning algorithm [14].

II. METHODS

The project will attempt to generate sky maps more efficiently and accurately, by 1) using abstract waveforms formulated by singular value decomposition and 2) utilizing machine learning techniques such as simulation based inference (SBI) that would reduce computational costs while producing a low-latency, sky map result. The project will use neural networks to connect

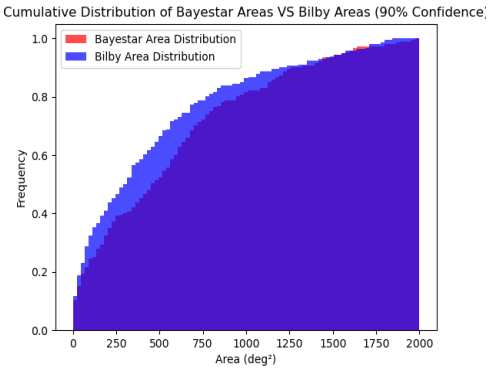

FIG. 4: A cumulative area distribution comparison of BILBY and BAYESTAR results. BILBY surpasses BAYESTAR with higher frequencies at smaller areas of degrees^2.

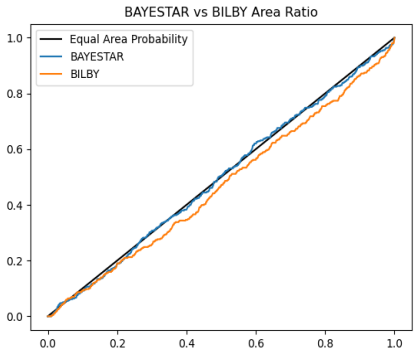

FIG. 5: The Probability-Probability (PP) plot visually compares the area percentiles of the two systems. A steeper line represents better localization accuracy, while a flatter line indicates worse accuracy.

abstract SNRs that are produced by SVD to the physical properties of GW candidates. sky maps will be computed from source localization and distance.

SVD SNRs will be ingested into a SBI motivated framework to compile a parameter estimation and demonstrate dimension probability. We will run simulations to train the algorithm, allow it to learn the shape of our current data, and build a posterior. From this, we can then compare simulated source parameters and test the validity of the posterior. Our final goal will be to construct an accurate sky map showing the 50% and 90% confidence areas of the sky where the source is located.

We researched two sky map algorithms. BAYESTAR, which computes low-latency sky maps by assuming a singular template [15], like represented in Figure 3, and BILBY, which takes many templates into account for a better localized sky map [16]. However, BILBY has a computing time on the order of hours to days. We extracted data in square degrees and compared the two systems in a 90% confidence areas. To filter data and study true results, criteria have been set at signal-to-noise signal greater than 9, and a false alarm ratio (FAR) less than 1 yr^{-1} or less than 2 yr^{-1}. We will also refer back to these systems with the project results as a comparison tool. BAYESTAR and BILBY data comes from mock data challenges (MDCs) that were run in the lead up to O4. MDCs look at all uploads done to a low-latency database and compares the two sets of sky maps.

In Figures 4 and 5, evidence shows that BILBY's complex computations can produce a more accurate sky map than BAYESTAR's low-latency algorithm. The project strives to achieve each system's strengths of low-latency and more accurate localization with the use of SVDs and machine learning.

III. RESULTS

By utilizing LALSuite, a public collection of gravitational wave software, we are able to set boundaries for each parameter and simulate injections with varying parameters to binary coalescence gravitational wave sources.

Due to the high level of dimensions applicable to binary coalescences, we began testing by setting all parameters in the LALApps configuration to fixed or 0, which allowed distance to be a free parameter, with boundaries of 100 to 1000 megaparsecs (mpc). Varying sample sizes from 10 000 injections (5000 from each interferometer) were processed to each include a varying distance and an SVD time-series, and added into a training network, which resulted in a posterior. Plotting posteriors demonstrated about 800 samples were needed to train the network to achieve accurate results. To test significance, we are using measured SVD responses for known sources and comparing how well our network predicts the true value. Randomly selected true distance values were displayed against posteriors. 27% of true values lied outside the predicted distribution (73% accuracy rate). Half of the true values that fell outside the posterior, were underestimated due to the parameter boundary in place, for there are signals that have been detected from distances further than 1000 mpc. If a larger distribution of distances were included in the training, posteriors would be underestimating true values at a smaller percentage.

After one dimensional training and plotting success, a second free dimension, inclination, was added to the injections. With a total of 10 000 injections, 3250 samples were used to draw accurate posteriors. Approximately 15% of true values fell outside inclination distribution while zero true values fell outside the distance distribution, giving us a total parameter accuracy rate of 85% accuracy rate. To check for possible bad data, more posteriors were creating using data from H1 only. Between

posteriors drawn from H1 solely and H1 and L1, distributions had an increase in variance for H1 and similar accuracy when predicting true values.

To set fourth our goal of an accurate sky map, the next trial included two localizing parameters, right ascension and declination. 60 000 total injections were created and 9000 samples were drawn to plot accurate posteriors. Out of 60 parameters in 4 dimensions, 23% of true values fell outside the posterior (77% accuracy rate). Initial observations from the 4 dimensional posteriors include the lacking stability of right ascension distribution. Even at an increased number of samples, there is a high variance for the distribution. In a few cases between 8000 and 10 000 samples, distance has a difficult time displaying a solidified distribution.

The posteriors drawn in first three trials have an average accuracy of about 78.3%, but the final goal is to reach a 90% accuracy rate. Furthermore, the precision of the distribution still struggles. Due to these observations, we plan to increase both precision and accuracy by adjusting the neural network input shape. Due to the formatting required by SBI, SVD data matrices were compressed into a one dimensional list. This formatting can forego some vital information about our data, where the framework can struggle with separating each waveform from the next. Adjustments were made to the neural network to preserve matrix structure, in hopes for better results in accuracy and precision.

After adjustments to the neural network, initial observations show an accuracy rate for various sample sizes of 83% or greater. Sample size of 15 000 represented the greatest accuracy and precision. Each distribution is mid-narrow in precision, with a total accuracy rate of 90%. Distance and declination are precise and accurate. We notice a bimodal variance for right-ascension distributions and uniform distributions for inclination. However, a bimodal distribution is excepted for inclination. These observations encourage more research into our data and processes for the inclination parameter.

The next steps of the project involve adjusting variables deeper into our neural network. After the network input adjustment, our neural network works as an image classifier, due to the matrix input shape. Convolutions neural networks (CNNs) are common in image classification and are used to categorize patterns and shapes. We will adjust 8 factors included in the CNN such as kernel size and learning rate, to achieve accurate posterior and sky map results.

IV. IMPLICATIONS

Data attainment and detection times have been minimized in recent research. Data interpretation still requires extreme expenses and efforts. The goal to calculate physical properties of the CBC from the abstract waveforms efficiently will allow a beginning to instantaneous review of possible overlaps in GW with EM data. This multi-messenger cooperation allows astronomers to view the universe through a lens never examined before.

[1] B. P. Abbott et al. (LIGO Scientific), Phys. Rev. D **95**, 062003 (2017), arXiv:1602.03845 [gr-qc].
[2] B. P. Abbott et al. (LIGO Scientific, Virgo), Phys. Rev. Lett. **119**, 161101 (2017), arXiv:1710.05832 [gr-qc].
[3] NASA ESA (2017).
[4] A. Levan et al., (2023), arXiv:2307.02098 [astro-ph.HE].
[5] R. Magee et al., Astrophys. J. Lett. **910**, L21 (2021), arXiv:2102.04555 [astro-ph.HE].
[6] B. P. Abbott, R. Abbott, T. D. Abbott, Abernathy, and others., .
[7] K. Cannon et al., Astrophys. J. **748**, 136 (2012), arXiv:1107.2665 [astro-ph.IM].
[8] A. Reza, A. Dasgupta, and A. S. Sengupta, (2021), arXiv:2101.03226 [gr-qc].
[9] K. Cannon, C. Hanna, and D. Keppel, Phys. Rev. D **84**, 084003 (2011), arXiv:1101.4939 [gr-qc].
[10] K. Cannon, C. Hanna, and D. Keppel, Phys. Rev. D **85**, 081504 (2012), arXiv:1108.5618 [gr-qc].
[11] J. Veitch et al., Phys. Rev. D **91**, 042003 (2015), arXiv:1409.7215 [gr-qc].
[12] V. Raymond, M. V. van der Sluys, I. Mandel, V. Kalogera, C. Rover, and N. Christensen, Class. Quant. Grav. **27**, 114009 (2010), arXiv:0912.3746 [gr-qc].
[13] K. Cannon, A. Chapman, C. Hanna, D. Keppel, A. C. Searle, and A. J. Weinstein, Phys. Rev. D **82**, 044025 (2010), arXiv:1005.0012 [gr-qc].
[14] R. Qiu, P. G. Krastev, K. Gill, and E. Berger, Phys. Lett. B **840**, 137850 (2023), arXiv:2210.15888 [astro-ph.IM].
[15] L. P. Singer and L. R. Price, Phys. Rev. D **93**, 024013 (2016), arXiv:1508.03634 [gr-qc].
[16] P. Baral, S. Morisaki, I. Magaña Hernandez, and J. Creighton, (2023), arXiv:2304.09889 [astro-ph.HE].